J Mater Sci (2011) 46:3470–3479
DOI 10.1007/s10853-011-5252-y

X-ray characterization of starch-based solid foams

Paavo A. Penttilä · Jussi-Petteri Suuronen · Satu Kirjoranta · Marko Peura · Kirsi Jouppila · Maija Tenkanen · Ritva Serimaa

Received: 18 November 2010 / Accepted: 6 January 2011 / Published online: 19 January 2011

Abstract Wide- and small-angle X-ray scattering (WAXS and SAXS) and X-ray microtomography were used to study the structure of brittle, solid foams made by extrusion of whole grain barley flour and additional whey protein isolate (WPI) and polydextrose (PD). The structure of the extrudates was described in a coarse way from nano- to microscale, and the effects of additives were discussed. The additives were observed to affect the structure in many scales, for instance, by inducing differences in the crystal structure of starch and in the microscale pore structure observed with both SAXS and X-ray microtomography. The most significant effects were introduced by WPI, but these were highly reduced in the presence of PD. Differences were also seen in lamellar structures of starch, which were probably formed due to retrogradation and observed with SAXS in powder samples soaked in water before the measurements.

Introduction

Extrusion cooking is a widely used technique for producing cereal-based solid foamy structures. The process consists of subsequent steps of mixing salt water with flour and cooking the mixture when transferring through a barrel by rotating screws. As the mass reaches the end of the barrel, it undergoes a rapid decrease in pressure, which causes an expansion of the mass [1].

The applications of starch-based solid foams are wide. In addition to their traditional applications in food products, they can be used as part of various composites or as starch plastics [2–5]. Because starch is cheap, abundantly produced, biodegradable, and available from renewable sources, it is a tempting alternative for oil-based plastics. Truly biodegradable starch plastics would be the ideal material for many disposable items [4]. In order to replace conventional commodity plastics such as polyethylene and polypropylene, the properties of starch-based plastics ought to be similar to theirs. These properties are ultimately dependent on the structure of starch at a crystalline level, which makes it highly important to understand the complicated structure in different length scales and its connection to the macroscopic properties of starch-based solid foams [6].

Starch consists of two types of molecules, the linear amylose (degree of polymerization—DP; 1500–6000) and branched amylopectin (DP 3×10^5 to 3×10^6) [7]. Amylose is formed of α-1,4-linked D-glucopyranose rings and amylopectin of amylose chains linked to each other with α-1,6-bonds at the branch points [8]. Native starch occurs in semi-crystalline granules, which consist of alternating amorphous and crystalline lamellae stacked in growth rings that are separated by larger amorphous regions. The sum of the thicknesses of one amorphous and one crystalline lamella ranges from 9 to 10 nm [8, 9], where the crystalline part makes a contribution of 5–7 nm [9]. Starch can be viewed in them as a side-chain liquid-crystalline polymer (SCLCP) [10, 11], where the amylopectin branching points mainly lie in the amorphous

Electronic supplementary material The online version of this article (doi:10.1007/s10853-011-5252-y) contains supplementary material, which is available to authorized users.

P. A. Penttilä (✉) · J.-P. Suuronen · M. Peura · R. Serimaa
Department of Physics, University of Helsinki, PO Box 64, 00014 Helsinki, Finland
e-mail: paavo.a.penttila@helsinki.fi

S. Kirjoranta · K. Jouppila · M. Tenkanen
Department of Food and Environmental Sciences, University of Helsinki, PO Box 66, 00014 Helsinki, Finland

lamellae [8]. The crystal structure found in most native cereal starches is A-amylose, which consists of intertwined sixfold left-handed parallel double helices, packed in a parallel fashion [8, 9, 12]. Another crystal structure, B-amylose, can be found in tubers and amylose-rich starches [8]. They are formed of double-helices of longer chain segments [9], packed in a less tight manner than A-amylose [12]. The granules present in barley starches can be divided in two [8, 9] or three [13] different categories according to their size. The average diameter of large (lenticular [9]) granules from normal barley is 15–25 μm and that of small (spherical [9]) granules 2–5 μm [8, 9, 13, 14].

Amylose may also co-crystallize with some compounds in a single-helical structure, generally known as V-amylose [8, 15]. The structure is a sixfold left-handed helix with a hydrophobic central cavity. The most studied V-type structure is Vh (hydrated amylose, also noted V_{6I} [16]), which is a presumably orthorhombic [16] structure of amylose–lipid complexes. The central cavity of the helix is most often assumed to be occupied by the aliphatic part of the lipid with its polar group lying outside, even though the location of the polar group is still being argued [16, 17]. A less studied amylose single-helical structure, named Eh, is stable at low moisture content [18]. Its diffraction pattern (with peaks at 7.0, 11.9, 13.2, and 18.1°; $\lambda = 1.5418$ Å [17]) has been attributed to a hexagonal unit cell consisting of helical amylose chains with 7 glucose units per turn (denoted also V_7) [6, 17]. In addition to larger, bulky complexing agents [6, 16], the sevenfold amylose helices have been found as complexes with lipids [17], which comprise about 1% of the dry weight of purified normal barley [8]. In native starch, amylose–lipid complexes can be present inside the granules or on their surface [16].

During extrusion, starch granules are irreversibly gelatinized and a mainly amorphous material, plasticized starch, is formed. However, the material rapidly organizes into so-called processing-induced crystal structures [2, 6]. This term refers to the single-helical crystal structures formed during processing (Vh and Eh), as distinct from the "residual crystallinity" from native starch (A and B) [2, 6]. The relative abundances of these are determined by the composition and source of the raw material and the processing parameters of the extrusion. For instance, the Eh structure has been shown to transform into the Vh form when the extrusion water content was increased, whereas an increase of extrusion temperature seemed to favor the Eh form [6, 19]. The amount of single-helical crystal structures in general can be increased by increasing the screw speed or the amylose content [4]. After extrusion, the crystal structure of starch may also change as a result of retrogradation [20], which is the form of aging above the T_g [2, 21].

The relative abundances of Vh and Eh crystal structures in extrusion cooked maize have been shown to correlate with the shape of the closed mm-sized air cells in two-dimensional images from optical microscope [19]. The extrudates with dominating Vh structure contained polyhedral cells, whereas those with Eh structure had more spherical-shaped cells. More recently, the properties of the 10–100 μm-sized cells, that is, the cell size and the cell wall thickness, have been studied with X-ray microtomography in different extrudates [1, 22–25]. The results suggest that cellular structures with larger cells also display thicker walls. Also connections of the structure in this scale to the expansion of the extrudates and their mechanical properties have been observed [1, 22].

The structure and properties of starch extrudates can be modified with different additives. Protein additives may change the rheological properties of extrusion mass by interacting between each other or with other molecules through cross-linking or bonding or they can affect the water distribution in the extrusion matrix, for instance, by forming insoluble aggregates [26]. Dietary fibers [27], at least when fibrous in their physical nature, may align in the direction of flow and, if soluble, bind some of the water present in the matrix. In higher concentrations, they may also disrupt the continuous structure of the extrudate melt [26].

In this study, we used whey protein isolate (WPI) and polydextrose (PD) to induce changes in the structure of starchy extrudates. WPI contains at least 90% whey protein [23], which is a mixture of globular, thermosetting proteins [24] created as by-products in cheese production [28] and supposed to be denatured under extrusion cooking conditions [29]. PD is a low-molecular weight, water-soluble, randomly bonded polysaccharide of glucose and it is used in foods to improve their structure and nutritional profile [1, 30]. PD as an additive in starch-based extrudates has not been widely studied. The effects of whey protein on expansion and microscale structure of starchy extrudates have been observed to be highly dependent on different extrusion parameters [1], protein content [23, 24, 31], and also on the source and manufacturing method of the protein [24]. For instance, the expansion of extrudates has been shown to both increase [23, 31] and decrease [24] with increasing level of WPI. Formation of insoluble complexes of whey protein with itself [32] and with amylose [28, 32] in extrusion of starchy materials has been observed. Also water-soluble, nanoscale ternary complexes formed by amylose, free fatty acids, and whey protein have been reported [33], but their self-assembly was highly disturbed already with a small amount of salt present in the solution.

Studies of starchy extrudates with combined small- and wide-angle X-ray scattering (SAXS and WAXS) have not been done widely, even though the combination of these methods may offer a picture of soft condensed matter in various length scales simultaneously [34–37]. X-ray

microtomography has proved to be an effective method in the study of cellular structures of brittle food foams [25]. In this work, we used SAXS, WAXS, and X-ray microtomography to study the structure of barley extrudates from nano- to microscale and the effects of added WPI and PD on it. Other characteristics of extrudates from the same series have been studied in an other publication [1].

Experimental

Extrusion

The main ingredient of the extrudates was fine whole grain barley flour (Mylly-Matti, Helsinki Mills Ltd., Finland), which was mixed with distilled water and salt (iodized salt, Meira Ltd., Finland) in the extruder. The salt (0.5% of solids) was dissolved in the water before mixing. Barley flour contained starch $67 \pm 3\%$, protein $10.5 \pm 0.1\%$, dietary fiber $12.1 \pm 0.7\%$, and β-glucan $3.5 \pm 0.1\%$ of solids. In addition, WPI (Isolate Whey 90 Instant, Armor Proteines, France) and PD (Litesse Ultra, Danisco Sweeteners, USA), in contents 20 and 10% of solids, respectively, were used as additives in some of the samples. The water contents of the ingredients were determined by drying them for 1 h in an oven (Termaks, Norway) at temperature of 130 °C, then cooling in a vacuum desiccator over phosphorus pentoxide (P_2O_5, pro-analysi, Merck, Germany) for 1 h and measuring the weight loss by using analytical balance (Precisa 92SM-202A, Teopal, Switzerland). These water contents were included in the water contents of the mass.

The extrusion was done with a co-rotating twin-screw extruder (Thermo Prism PTW24, Thermo Haake, Polylab System, Germany). The length of the screws was 672 mm and their diameter 24 mm (L/D ratio 28:1). The extruder barrel had altogether 7 sections, length of each 96 mm, the temperatures of which followed the profile: no warming, 40, 70, 70, 100, 110, and 130 °C. A heatable die (diameter 5 mm) was placed after the last section and it was kept at the temperature of the last section (130 °C). Total mass feed was kept constant at 67 g/min. Samples with two different water contents and screw speeds were extruded. Their additives and extrusion parameters are presented in Table 1. The samples were stored in sealed plastic bags at room temperature and normal humidity for some months before the first X-ray measurements.

Table 1 Additives and extrusion parameters of the samples

Sample no.	Additives	Water content (%)	Screw speed (rpm)
1	–	17	500
2	PD	17	500
3	WPI	17	500
4	PD + WPI	17	500
5	WPI	23	200
6	PD + WPI	23	200

WAXS measurements

Pieces of the extrudates were ground with a mortar into fine powder, pressed into metal rings of a thickness of 1.5 mm, and covered with Kapton or Mylar foil. The WAXS measurements were carried out with a system including an X-ray generator (UltraX18S, Rigaku, Japan) with a rotating Cu anode ($\lambda = 1.541$ Å) and an image plate detector (MAR345, Marresearch, Germany) in perpendicular transmission geometry. The beam was monochromated with a Si(111) crystal and a totally reflecting mirror. Corrections for absorption, measurement geometry, scattering by air and Kapton or Mylar foils, and the noise caused by the image reading process of the detector were carried out for the data. The measurements were repeated after 1–3 months with other samples from the same extrusion series, which gave diffraction patterns practically identical to those from the first measurements.

SAXS measurements

Materials and methods

SAXS measurements were carried out for dry and wet samples. The dry samples were prepared similarly to those for the WAXS measurements. For the wet samples, the powder was soaked in water for 2–3 days before removing the excess water and placing the swollen powder in metal rings. All of the samples in SAXS measurements were sealed with polypropylene foil.

The radiation was produced with an X-ray generator (K 710 H, Siemens, Germany) and an X-ray tube with a Cu anode (Panalytical, Netherlands), monochromated and point-collimated, and detected with a two-dimensional wire detector (HI-STAR, Bruker AXS, USA) in perpendicular transmission geometry. The measured q range was 0.016–0.21 $Å^{-1}$, where the definition $q = (4\pi \sin\theta)/(\lambda)$, with θ being half the scattering angle, was used for the magnitude of the scattering vector. Spatial and flood-field corrections for the data were done automatically by the measurement program. The air scattering was measured with an empty polypropylene-covered ring and subtracted from the integrated intensities. The intensities were calibrated on absolute scale using a piece of Lupolen as standard [34, 38].

Data analysis

The Porod law ($I(q) \propto q^{-4}$) is valid for a system with two phases separated by a smooth interface. With the knowledge of the volume fractions and electron densities of the phases, the specific surface of the system, that is, the surface area per mass unit of the solid material, can be calculated using this Porod fit. Porod law can also be used to calculate average chord lengths, which describe the distances between interfaces in the system averaged in all directions. These can also be specified for the phases separately [34, 39, 40]. The two phases were assumed to be solid material, including crystalline and amorphous starch, and air-filled pores (scattering length density contrast $\Delta\rho = 1.4 \times 10^{11}\,\mathrm{cm}^{-2}$) in the dry samples and crystalline starch and water ($\Delta\rho = 4.5 \times 10^{10}\,\mathrm{cm}^{-2}$), the latter including both the water-filled pores and regions of swollen amorphous starch, in the wet samples. These assumptions are discussed more in "Discussion" section. See Supplementary material 1 for the equations and a more detailed description on the calculations.

SAXS intensities can show power laws of the form $I(q) \propto q^{-\alpha}$ also with other powers than $\alpha = 4$. Such behavior indicates fractal-like (or self-similar) structures in the corresponding length scale ($d = 2\pi/q$), so that powers $\alpha \leq 3$ correspond to mass fractals of fractal dimension $D_m = \alpha$ and powers $3 < \alpha < 4$ to surface fractals of fractal dimension $D_s = 6 - \alpha$. Generally, aggregated structures with surface fractals are denser inside than those with mass fractals and a smaller mass fractal dimension corresponds to a less compact structure. The special cases of integer powers $\alpha = 1$ and $\alpha = 2$ correspond to rod-like and lamellar structures, respectively [34, 41, 42].

Microtomography measurements

The X-ray microtomography (μCT) measurements were carried out using a high-resolution X-ray microtomography device (Nanotom 180NF, phoenix|x-ray Systems + Services GmbH, Germany). The device consists of an end-window type tungsten target X-ray tube, a high-precision computer-controlled translation/rotation stage for the sample and a CMOS flat panel X-ray detector with 2304 × 2284 pixels of 50 μm size (Hamamatsu Photonics, Japan). Small pieces of approximately 0.5 × 0.5 × 0.5 mm^3 were cut from the dry extrudates with a razor blade and attached with beeswax on a carbon fiber rod. The measurements consisted of 1440 X-ray transmission images, taken at 0.25° intervals around a full circle of rotation. The X-ray tube voltage was 60 kV, and the current was varied between 200 and 360 μA. Because the samples were mounted very near the focal spot of the X-ray beam in cone-beam geometry, the effective pixel size in the transmission images varied between 450 and 766 nm. The 3D reconstructions were made using the datos|x-rec software supplied by the μCT device manufacturer. Scans made from whole extrudates with a larger voxel size have been described in an other publication [1].

Results

SAXS results

SAXS intensities of dry and wet samples are presented in Figs. 1 and 2, respectively. The Porod fit was done for all samples on higher q values, that is above 0.13 and 0.16 $\mathrm{Å}^{-1}$ for most of the dry and wet samples, respectively (see Figs. S1 and S2 in Supplementary material 1). The specific surfaces and the average chord lengths could be calculated only for the dry samples (Table 2) because of difficulties in determining the volume fractions in the wet samples and the shortness of the range of the Porod fit. The error estimates in Table 2 are based on variation of the region of the Porod fit.

The intensities of the dry samples obeyed power laws in region $q = 0.016 - 0.07\ \mathrm{Å}^{-1}$, which corresponds to structures of 10–40 nm. The wet samples showed two power law regions, one on smaller q values ($q = 0.016 - 0.045\ \mathrm{Å}^{-1}$; $q = 0.025 - 0.065\ \mathrm{Å}^{-1}$ for Sample 6) and one on larger q values ($q = 0.045 - 0.16$ Å; $q = 0.065 - 0.16\ \mathrm{Å}^{-1}$ for Sample 6). The corresponding fractal dimensions D_s (dry samples), D_{m1} (wet samples, small q), and D_{m2} (wet samples, large q) are presented in Table 2. Before determining the power laws, a small

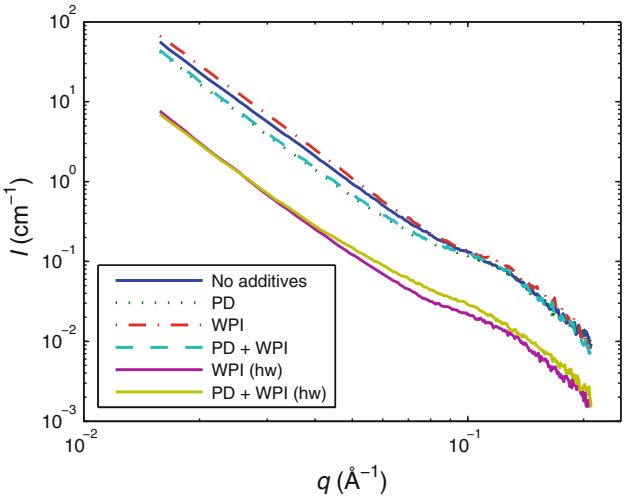

Fig. 1 SAXS curves of the dry samples, with correction from Porod law subtracted and curves of samples with higher water content (hw) multiplied by 0.2 for clarity

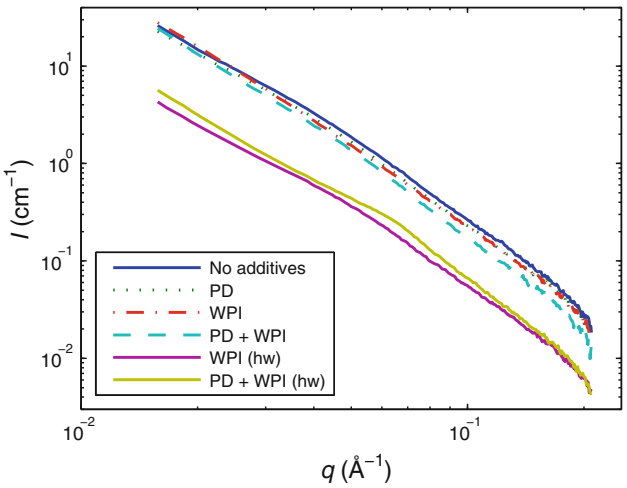

Fig. 2 SAXS curves of the wet samples, with correction from Porod law subtracted and curves of samples with higher water content (hw) multiplied by 0.2 for clarity

constant b gained from the least-square fit of $I(q) = aq^{-4} + b$ (Porod fit) to the data was subtracted from the data. The constant was of order 10^{-2} cm^{-1} for all samples and it corrects especially for the constant background due to water in the wet samples. The error estimates for all fractal dimensions were determined to be less than 0.1 by varying the fitting ranges.

Some effects introduced by the additives were observed in the dry Samples 1–4 (Table 2). The addition of WPI alone increased the specific surface by 20% (Sample 3), whereas the values of the samples with PD (Samples 2 and 4) were similar to the reference sample (Sample 1), independent of WPI content. The same trends were reflected in the average chord lengths, where the addition of WPI alone (Sample 3) decreased the length. The average size of air-filled pores (L_p) increased with the addition of WPI alone (Sample 3), but the additional presence of PD (Sample 4) reduced the effect to minimum. Addition of PD alone (Sample 2) slightly decreased the pore size compared to the reference. Opposite trends applied to the average chord lengths of the solid phase (L_s).

The macroscopically denser Samples 5 and 6, produced with higher water content and slower screw speed, showed different kind of behavior relative to the additives. The sample with only WPI added (Sample 5) had smaller specific surface but larger pore size than the sample with both WPI and PD added (Sample 6), and their average chord lengths of the solid phase were equal. This already shows that water content of extrusion mass and the screw speed affect the way the additives change the structure of barley extrudates on several levels, because the specific surfaces arise from nanoscale structures and the observed average chord lengths reflect structures of micrometer scale. A rougher surface structure of the dry Samples 5 and 6 can be seen in their surface fractal dimensions (D_s; Table 2), which correspond to the length scale of tens of nanometers.

The SAXS data were also interpreted according to a lamellar model. To emphasize the contribution of possible lamellar peaks, the data were drawn as q^2I versus q, which showed lamellar structures in almost all of the samples. Among the wet samples (Fig. 3), especially Samples 5 and 6 had clearly visible peaks around $q = 0.04$ Å^{-1} and $q = 0.06$ Å^{-1}, respectively. The peak of Sample 6 corresponds to an interlamellar distance of approximately 10 nm, which is usually attributed to the alternating crystalline and amorphous lamellae of amylopectin in hydrated starch [9]. The peaks of the other samples, however, arise from larger lamellar structures (e.g. 15 nm for Sample 5). An obvious similarity between the shapes of the curves of the samples without WPI (Samples 1 and 2) was also evident and their lamellar peaks were on smaller q values. Unlike the wet samples, the dry samples all showed a weak lamellar peak corresponding to an interlamellar distance of 5 nm, which is also visible as a shoulder in Fig. 1.

The power laws of the wet samples indicated less compact structures than those observed for the dry samples. The mass fractal dimensions on the larger q values (D_{m2})

Table 2 SAXS results

Sample	Additives	S (m^2/g)	L_c (μm)	L_p (μm)	L_s (μm)	D_s (dry)	D_{m1} (wet)	D_{m2} (wet)
1	–	1.03 ± 0.05	0.60 ± 0.07	1.0	1.5	2.5	2.2	2.84
2	PD	0.99 ± 0.05	0.59 ± 0.07	0.9	1.7	2.5	2.2	2.85
3	WPI	1.22 ± 0.12	0.47 ± 0.07	1.4	0.7	2.4	2.5	2.79
4	PD + WPI	0.99 ± 0.10	0.61 ± 0.09	1.0	1.5	2.4	2.4	2.96
5	WPI	0.94 ± 0.07	0.66 ± 0.08	1.7	1.1	2.6	2.1	2.80
6	PD + WPI	1.21 ± 0.06	0.53 ± 0.06	1.0	1.1	2.8	2.0	3.04

S specific surface, L_c average chord length, L_p average chord length of pores (±0.1 μm), L_s average chord length of solid (±0.1 μm), D_s surface fractal dimension, D_{m1} mass fractal dimension (smaller q values, wet samples), D_{m2} mass fractal dimension (larger q values, wet samples)

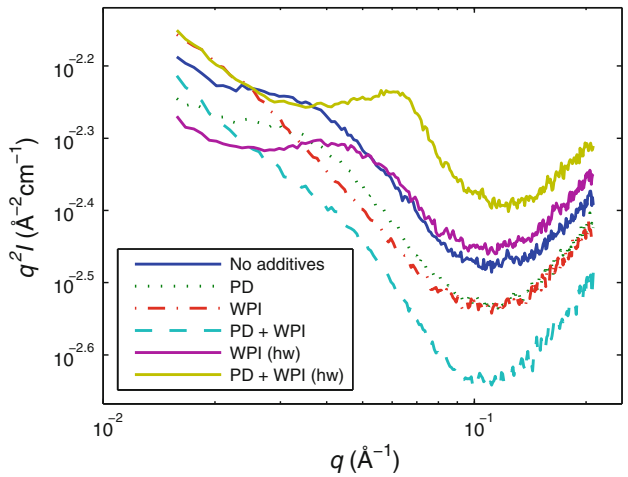

Fig. 3 SAXS curves of the wet samples (hw = higher water content) drawn on (q, q^2I) coordinates to enhance the lamellar peaks

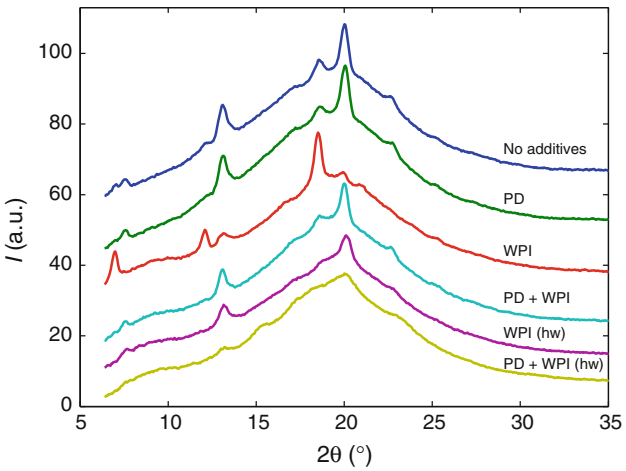

Fig. 4 WAXS curves of all samples (hw = higher water content), taken from the later measurements done about 1 year after extrusion and offset for clarity

correspond to more compact structures than those on smaller q values (D_{m1}). A characteristic length, where the type of the structure causing the scattering possibly changes, could be deduced from the turnover point in the curves of Fig. 2, that is, where the power law changes. This yields the length 14 nm (9.7 nm for Sample 6). The mass fractal dimensions of wet Samples 3 and 4 on smaller q values (D_{m1}) were slightly higher than those of Samples 1 and 2, which indicate a denser or less-lamellar structure for wet samples with WPI in this length scale.

WAXS results

The WAXS curves of all samples are presented in Fig. 4. They show a partly crystalline material with an amorphous contribution seen as a slowly varying background. Separate diffraction peaks arising from crystalline starch are more or less visible in all of the samples. The peaks of Samples 1, 2, 4, and 5 can be recognized to correspond mainly to the Vh-type structure (peaks at $2\theta = 7.6°$ ($hkl = 110$ [43]), $2\theta = 13.1°$ (200 or 021 [43]), and $2\theta = 20.0°$ (150 [43])), whereas Sample 3 shows the characteristic peaks of the Eh-type structure (peaks at $2\theta = 7.0°, 2\theta = 12.1°$, and $2\theta = 18.5°$) [6]. However, all of the samples show characteristics of both crystal structures. Sample 6 is clearly more disordered than any of the other samples, but it seems to contain slightly more Vh-type than Eh-type.

Tomography

Examples of X-ray μCT images, filtered using the gaussian smoothing and edge-preserving smoothing filters of Avizo Fire software, are presented in Figs. 5, 6, and 7. The main point of interest in the μCT results is the presence of some remaining starch granules in all samples. These are seen in

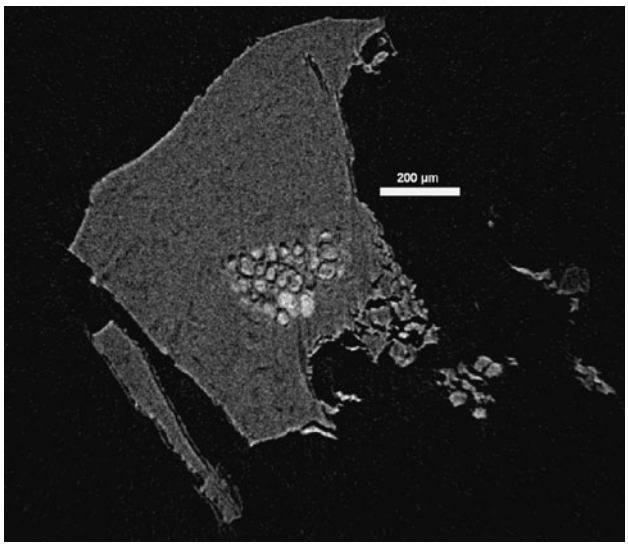

Fig. 5 A slice through the μCT reconstruction of Sample 2 (PD added) with voxel size of the scan 648 nm

the μCT images as spherical objects that are somewhat denser than the surrounding material. The size of the objects varies from a few microns to around 20 μm in diameter, which is consistent with observations on barley starch granules found in the literature [13]. As can be seen from the figures, most of the remaining granules are clustered together, although some individual granules were also observed embedded in the surrounding material. As a crude approximation based on manual segmentation of the data, the granules comprise 1–2% of the total sample volume. Dual threshold segmentation of the data from scans of intact extrudates also yielded the same result.

The μCT images also show some inhomogeneity in the solid mass surrounding the granules, as shown in Fig. 7.

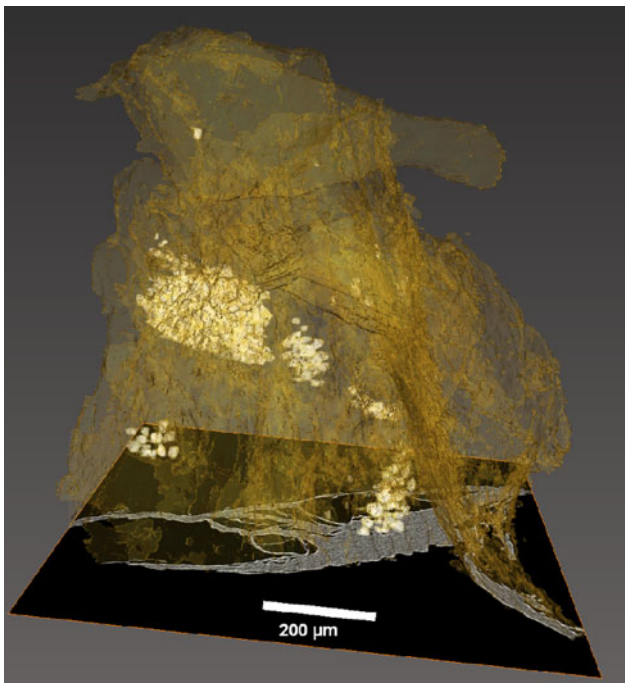

Fig. 6 A 3D rendering of Sample 3 (WPI added) with the starch granules rendered in white, showing their clustered distribution within the sample (voxel size 682 nm)

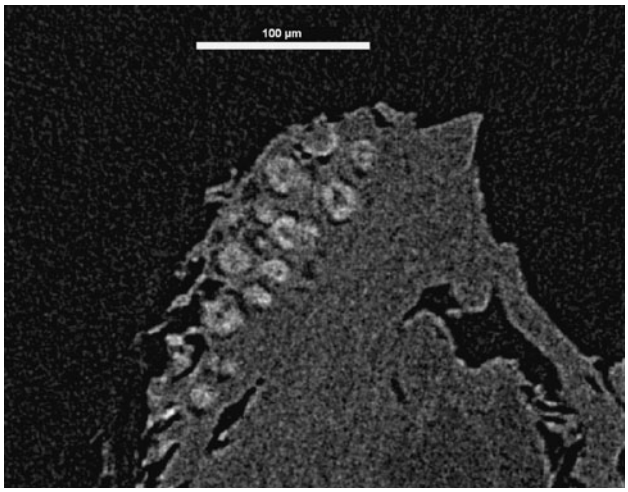

Fig. 7 A slice through the µCT reconstruction of Sample 3 (WPI added) with voxel size 450 nm

Structures of the same scale were observed in the average chord lengths of the SAXS results, which showed the average chord lengths of the solid phase to be roughly the same as one voxel in the µCT reconstruction and the average chord length of the voids to be slightly larger. It would be reasonable to assume that these structures are also visible in the µCT images as slight variations in gray value, although they are too small to be completely resolved at a voxel size of several hundred nanometers.

Discussion

General structure of the extrudates

The results of the microtomography and SAXS measurements of this work can be explained with the structure sketched in Fig. 8. The millimeter or 100 µm scale structure, which can be seen with optical microscopy or X-ray microtomography with low resolution [1], is formed of a foamy solid material with irregularly shaped air-filled pores. The shape of the pores did not follow the type of crystal structure, as earlier presented by Warburton et al. [19], but this was explained by Babin et al. [22] by the rapidity of the setting process. In Samples 5 and 6, these pores were minimal or very few and the samples mostly consisted of solid material in this scale. The presence of intact granules in the high-resolution microtomography images is not surprising, because starch gelatinization does not happen instantaneously [44], and the water distribution inside the mass during extrusion is not uniform [1]. Granule remnants consisting of the outer portion of the granule only can also remain after cooking under no to moderate shear [27]. Surrounding the granules, smaller structures were seen in the matrix. These structures could be µm-sized air-filled pores, giving rise to the main proportion of the specific surface and thus the average chord lengths obtained from the SAXS measurements (Table 2). The surface fractal dimensions of $D_s \approx 2.5$ in the scale of 10–40 nm could arise from the surfaces of these pores and other structures on the same length scale. The dominating crystal structure in the samples is one of the typical processing-induced crystals, Vh or Eh, even though the granules may include some residual A-type crystallinity. In Sample 6, the crystalline fraction is particularly low.

Similar SAXS results have been gained, for instance, by Suzuki et al. [42], who studied corn and potato starch

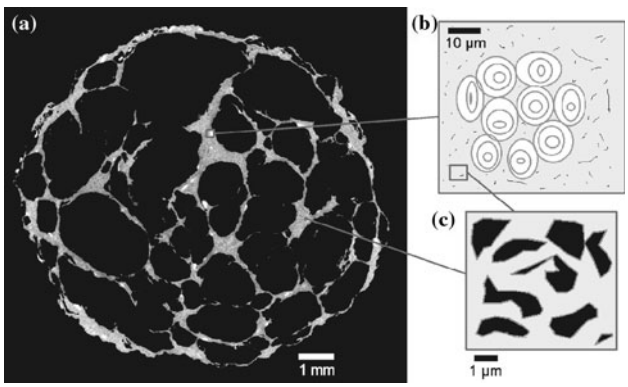

Fig. 8 Sketch of the structure of the extrudates: **a** cross section of an extrudate (Sample 1, no additives), **b** small cluster of granules, **c** air-filled micropores inside the solid matrix

during swelling, gelatinization, and retrogradation, and interpreted the power law behaviour of intensity curves on the basis of fractal structures. Their intensities of dry and low-moisture corn starch obeyed power laws with surface fractal dimensions close to 2.0 on a wide q range, which also comprises the length scale of our power laws. They explained these power laws by the surface fractal structure of granules, but since in our case the proportion of granules in the samples was relatively small, it is plausible that this behavior arises from the microporous structure in the matrix, which was observed in the microtomography images and in the average chord lengths of the SAXS results. Lopez-Rubio et al. [36] also found a power-law with α close to 4 in high-amylose maize starch and observed a decrease of α upon extrusion. They attributed this effect to increased surface roughness of the scattering structures.

A shoulder or weak lamellar peak representing a distance less than 9 nm has been observed earlier in some SAXS studies on dry starch, in which it has been attributed, for instance, to amylose crystals formed during enzymatic digestion (5 nm repeating distance) [36, 37] or crystalline lamellae of chain-folded amylose–lipid helices in spherulitic amylose–lipid complexes (7–8 nm repeating distance) [17]. Also the 5-nm shoulder of our dry SAXS curves could arise from these kinds of amylose-based structures. However, as indicated by the amorphous WAXS pattern of Sample 6, the presence of this feature does not require a large proportion of crystalline material.

In the dry samples, it was assumed that the main proportion of the small-angle scattering arises from the interface between starch (including both crystalline and amorphous portions) and air [42]. However, this approximation is never completely valid, and an electron density difference between different solid phases is always present. In the wet samples, the effects of water on the system have to be taken into account with further assumptions. In order to be able to consider a two-phase system, Suzuki et al. [42] assumed that the water absorbs to the amorphous regions so that the electron density difference relevant for SAXS forms between the crystalline and the amorphous parts in starch granules.

The values of specific surfaces and average chord lengths presented in Table 2 may contain systematic error due to the notable amount of parameters to be approximated, but this should not affect the comparability of the values between each other. For instance, the density of the solid phase, needed in the calculation of the scattering length densities, was assumed to be 1.55 g/cm^3 for all samples, whereas Babin et al. [22] used a density of 1.405 g/cm^3 for amorphous starches at 10% moisture content. Such deviation in density has been noticed to have an effect of tens of percents on the eventual values and is discussed in more detail elsewhere [34]. Here, the use of density 1.50 g/cm^3 would have increased the specific surfaces of all samples by about 10%, which would not affect the interpretation of our results.

Our SAXS data of the wet samples showed mass fractal dimensions between 2.0 and 3.0 as well as lamellar peaks or shoulders, that resemble those observed by Suzuki et al. [42] in their retrograded potato starches. Their samples were prepared by keeping them in 1:1 water–solid ratio at 4 °C for 1–2 days after gelatinization. Despite that their curves included several regions with slightly different power laws, looking fairly similar to ours on the common q range, they proposed a background fractal scattering following a mass fractal dimension of 1.9 on the whole region. According to them, the additional shapes and the shoulder-like pattern at 0.02–0.04 Å^{-1} would arise either from a new, large lamella stacking caused by retrogradation or two completely different fractal scattering regions at high and low q values. A similar shoulder was detected by Lopez-Rubio et al. [36] in extruded high-amylose maize starch soaked in water for 1 h. They concluded that the 9-nm peak of raw starch was lost, and a broad shoulder on smaller q values was formed due to a retrogradation process taking place upon addition of water.

The transition of the crystal structure of starch from V-type to B-type due to addition of water has been observed earlier [45], and the lamellar peak in the wet samples might be explained by the repeating distances in a fractal-like network of B-type crystals and amorphous amylose, a system characterized with TEM by Putaux et al. [46]. This would give a connection between the WAXS pattern and wet SAXS peak of Sample 6: the amorphous amylose chains are more easily organized into B-type crystals and thus ordered lamellae in water than the samples with more crystallized amylose–lipid complexes. On the other hand, complexes of amylose and native lipids of cereal starch granules have also been shown to form fractal-like structures of crystalline aggregates during slow cooling of jet cooked starches in dilute solutions [47].

Vermeylen et al. [44] studied the gelatinization of waxy rice, regular rice, and potato starch suspensions (66% water content) with real-time SAXS and WAXS during heating. They found mass fractals of dimensions 1.5–1.8 for fully gelatinized starch pastes on the same q range as our low-q power laws (common q range 0.016–0.035 Å^{-1}), and they accounted them for fractal-like structures formed by amylose. In partly gelatinized systems, they recognized fractal-like structures, α decreasing with temperature, and possible residual lamellar stacks (with repeating distance of 9-10 nm), present simultaneously. These kinds of lamellar peaks have also been observed in processed starch samples

(45% water content) without a detectable amount of original crystallinity [35].

Besides the lamellar model adopted in this work, SAXS data of complex polymer systems can be interpreted according to other models. An alternative approach would have been the model of De Spirito et al. [48], which interprets SAXS data in terms of the superimposition of scattering from spherical nano-sized particles distributed in space with a certain mass fractal dimension and from surfaces of larger particles.

The importance of the extrusion parameters was undeniable. Based on a visual examination of the extrudates and the low-resolution microtomography images (not presented), it seems obvious that Samples 5 and 6, which were extruded using higher water content of mass and lower screw speed, had undergone a collapse of bubbles after expansion. They had a significantly denser macroscopic structure and contained very few, if any mm-sized pores. This collapse is explained by the lower viscosity of the extrudate melt due to higher water content, which leads to a shrinkage and collapse of the extrudate [26].

Effects of additives

A key point in analyzing the differences caused by the additives is the interaction behavior of whey proteins. It has been shown that proteins can bond with each other or other molecules in extrudates, which leads to the formation of an extensive network [26]. Thus, our proposition is that whey protein, when present alone, formed an insoluble complex either with itself [32], with amylose [28, 32], or with some of the fibers or other ingredients present in whole grain flour [1]. During extrusion, the insoluble network affected the water distribution in the extrudate melt, possibly by leaving large amounts of water free to evaporate at the die. The especially high loss of water content during expansion in the sample with only WPI added (Sample 3) was observed in earlier measurements [1]. This explains also why the water content of Sample 3 after expansion was not high enough for the formation of the Vh-type crystal structure, which is more abundant at higher water contents [6, 19]. Instead, the Eh-type was seen to dominate the diffraction pattern of this particular sample. On a larger scale, whey protein had an influence on the micrometer scale pore structure, so that Sample 3 showed larger specific surface and larger pores with thinner walls.

Compared to whey protein, the effects of PD were minor. Samples 1 and 2, with the only difference in PD content, showed very similar results with all of our methods, even though variation was seen earlier in expansion properties and in the pore structure above micrometerscale [1]. Sample 1 contained, for instance, a higher proportion of thin ($<150\,\mu m$) walls compared to Sample 2 [1], which might be connected with its slightly smaller average chord length of solid sections (Table 2). However, in this study, PD affected the structure of the extrudates when it was combined with WPI by significantly reducing the effects introduced by WPI alone. This might be accounted for an interaction between PD molecules and whey proteins, which probably led to an inhibition of the formation of the protein-based network. A similar effect has been observed earlier in a starch–protein–polydextrose system, where PD was seen to break the protein matrix surrounding starch granules [30]. On the other hand, soluble fibers can affect the water distribution directly by binding some of the water in the matrix and affect the structure in that way [26, 49].

Interestingly, a connection between microscale wall thicknesses determined from lower resolution microtomography images [1] and the SAXS curves of this work was observed. The sequence in intensity of the SAXS curves of Samples 1–4 on smaller q values (larger structures) in all of our SAXS results, whether dry or wet, followed the sequence of the wall thicknesses of the same samples on smallest microscale wall thicknesses.

Based on the SAXS measurements of the wet samples, WPI also affected the retrogradation behavior of starch. In Fig. 3, the greatest differences in the peak positions between Samples 1–4 and their fractal dimensions D_{m1} in Table 2 are due to the presence of WPI, almost regardless of PD content. According to their D_{m1}'s deviating more strongly from 2.0 and peaks located on smaller q values, the samples with WPI show less ordered lamellae with larger interlamellar distance. Of course the differences may also be explained by the different structures of the samples already before immersing them in water.

The outer surface of the extrudate may differ in its structure from the inner parts and might as well contribute to all our X-ray scattering results because the whole cross sections of the extrudates were ground when preparing samples for the measurements. Such a difference was observed visually especially in Sample 3, which had a less porous layer on the surface. A similar effect, named the "skin effect" and obtained under certain conditions, has been reported earlier [31].

Conclusions

The structure of barley extrudates and effects of WPI and PD on it were studied using X-ray scattering and microtomography. The structure of the extrudates was described in a rather coarse way from nano- to microscale. The complex nature of the system made of the ingredients of whole grain barley flour, water, and the additives sets such great challenges that a full understanding of it is impossible. In addition to the large amount of different components in the

system, their interactions are largely affected by the ambient conditions, by which we mean the parameters of extrusion, as well as the conditions during storage.

However, we were able to propose some mechanisms, how the structure of the extrudates may have been affected by the different additives. We concluded that in the presence of whey protein as the only additive in extrusion with lower water content of mass and higher screw speed, an insoluble protein-based network was formed. Due to this network, the expansion of the extrudate was high and a large amount of water evaporated at the die, leading to a processing-induced crystal structure usually present at low water contents. The effects of PD were minor when present as the only additive, but it reduced the effects of whey protein, when these were present simultaneously. This was accounted for the destructive effect of soluble molecules on the insoluble protein-based network. The additives also influenced the lamellar structures found in the wet samples. It is proposed that these structures were formed due to retrogradation of starch when soaked in water. A more detailed description would require X-ray scattering experiments with a microfocus beam and imaging with higher resolution.

Acknowledgements The authors thank Tekes, The Finnish Funding Agency for Technology and Innovation, Academy of Finland (project 127759), and University of Helsinki Research Funds for financial support.

References

1. Kirjoranta S, Solala K, Suuronen J-P, Penttilä P, Peura M, Serimaa R, Tenkanen M, Jouppila K, Effects of process variables and addition of polydextrose and whey protein isolate on the properties of barley extrudates. LWT—Food Sci Technol (submitted)
2. Avérous L, Halley PJ (2009) Biofuels Bioprod Biorefin 3:329
3. Le Corre D, Bras J, Dufresne A (2010) Biomacromolecules 11:1139
4. van Soest JJG, Vliegenthart JFG (1997) Trends Biotechnol 15:208
5. Zhao R, Torley P, Halley PJ (2008) J Mater Sci 43:3058. doi:10.1007/s10853-007-2434-8
6. van Soest JJG, Hulleman SHD, de Wit D, Vliegenthart JFG (1996) Ind Crop Prod 5:11
7. Zobel HF (1988) Starch/Staerke 40:44
8. Buléon A, Colonna P, Planchot V, Ball S (1998) Int J Biol Macromol 23:85
9. Tester RF, Karkalas J, Qi X (2004) J Cereal Sci 39:151
10. Daniels DR, Donald AM (2004) Macromolecules 37:1312
11. Waigh TA, Gidley MJ, Komanshek BU, Donald AM (2000) Carbohydr Res 328:165
12. Popov D, Buléon A, Burghammer M, Chanzy H, Montesanti N, Putaux J-L, Potocki-Véronèse G, Riekel C (2009) Macromolecules 42:1167
13. Tang H, Watanabe K, Mitsunaga T (2002) Carbohydr Polym 49:217
14. Vasanthan T, Bhatty RS (1996) Cereal Chem 73:199
15. Gessler K, Usón I, Takaha T, Krauss N, Smith SM, Okada S, Sheldrick GM, Saenger W (1999) Proc Natl Acad Sci USA 96:4246
16. Putseys JA, Lamberts L, Delcour JA (2010) J Cereal Sci 51:238
17. Shogren RL, Fanta GF, Felker FC (2006) Carbohydr Polym 64:444
18. Mercier C, Charbonniere R, Grebaut J, de la Gueriviere JF (1980) Cereal Chem 57:4
19. Warburton SC, Donald AM, Smith AC (1992) J Mater Sci 27:1469. doi:10.1007/BF00542905
20. van Soest JJG, Knooren N (1997) J Appl Polym Sci 64:1411
21. Pushpadass HA, Hanna MA (2009) Ind Eng Chem Res 48:8457
22. Babin P, Della Valle G, Dendievel R, Lourdin D, Salvo L (2007) Carbohydr Polym 68:329
23. Cheng EM, Alavi S, Pearson T, Agbisit R (2007) J Texture Stud 38:473
24. Cho KY, Rizvi SSH (2009) Food Res Int 42:595
25. Trater A, Alavi S, Rizvi S (2005) Food Res Int 38:709
26. Moraru CI, Kokini JL (2003) Compr Rev Food Sci Food Saf 2:147
27. BeMiller JN, Whistler RL (1996) In: Fennema OR (eds) Food chemistry. 3rd edn. CRC Press, Boca Raton, FL
28. Matthey FP, Hanna MA (1997) Lebensm-Wiss Technol 30:359
29. Onwulata CI, Konstance RP, Cooke PH, Farrel HM Jr (2003) J Dairy Sci 86:3775
30. Stowell JD (2009) In: Cho SS, Samuel P (eds) Fiber ingredients. CRC Press, Boca Raton, FL, pp 173–201
31. Alavi SH, Gogoi BK, Khan M, Bowman BJ, Rizvi SSH (1999) Food Res Int 32:107
32. Allen KE, Carpenter CE, Walsh MK (2007) Int J Food Sci Technol 42:953
33. Zhang G, Maladen M, Campanella OH, Hamaker BR (2010) J Agric Food Chem 58:9164
34. Penttilä PA, Várnai A, Leppänen K, Peura M, Kallonen A, Jääskeläinen P, Lucenius J, Ruokolainen J, Siika-aho M, Viikari L, Serimaa R (2010) Biomacromolecules 11:1111
35. Chanvrier H, Uthayakumaran S, Appelqvist IAM, Gidley MJ, Gilbert EP, López-Rubio A (2007) J Agric Food Chem 55:9883
36. Lopez-Rubio A, Htoon A, Gilbert EP (2007) Biomacromolecules 8:1564
37. Lopez-Rubio A, Flanagan BM, Shrestha AK, Gidley MJ, Gilbert EP (2008) Biomacromolecules 9:1951
38. Vainio U, Maximova N, Hortling B, Laine J, Stenius P, Simola LK, Gravitis J, Serimaa R (2004) Langmuir 20:9736
39. Porod G (1982) In: Glatter O, Kratky O (eds) Small angle X-ray scattering. Academic Press, London
40. Spalla O, Lyonnard S, Testard F (2003) J Appl Crystallogr 36:338
41. Schmidt PW (1991) J Appl Crystallogr 24:414
42. Suzuki T, Chiba A, Yano T (1997) Carbohydr Polym 34:357
43. Zobel HF, French AD, Hinkle ME (1967) Biopolymers 5:837
44. Vermeylen R, Derycke V, Delcour JA, Goderis B, Reynaers H, Koch MHJ (2006) Biomacromolecules 7:2624
45. Zobel HF (1988) Starch/Staerke 40:1
46. Putaux JL, Buléon A, Chanzy H (2000) Macromolecules 33:6416
47. Fanta GF, Felker FC, Shogren RL (2002) Carbohydr Polym 48:161
48. De Spirito M, Missori M, Papi M, Maulucci G, Teixeira J, Castellano C, Arcovito G (2008) Phys Rev E 77:041801
49. Yanniotis S, Petraki A, Soumpasi E (2007) J Food Eng 80:594